Structural, magnetic, electronic and transport properties of $NdCu_2$

1991 J. Phys.: Condens. Matter 3 9297

(http://iopscience.iop.org/0953-8984/3/47/004)

J. Phys.: Condens. Matter 3 (1991) 9297–9318. Printed in the UK

Structural, magnetic, electronic and transport properties of $NdCu_2$

E Gratz†, M Loewenhaupt‡, M Divis§, W Steiner||, E Bauer†, N Pillmayr†, H Müller†, H Nowotny¶ and B Frick††

† Institut für Experimentalphysik, Technische Universität Vienna, A-1040 Wien, Austria

‡ Institut für Festkörperforschung, Forschungszentrum Jülich, D-5170 Jülich, Federal Republic of Germany

§ Department of Metal Physics, Charles University Prague, 12116 Prague 2, Czechoslavakia

|| Institut für Angewandte und Technische Physik, Technische Universität Vienna, A-1040 Wien, Austria

¶ Institut für Theoretische Physik, Technische Universität Vienna, A-1040 Wien, Austria

†† ILL Grenoble, F-38042 Grenoble Cédex, France

Received 8 July 1991

Abstract. $NdCu_2$ crystallizes in the orthorhombic $CeCu_2$ structure. Using temperature dependent x-ray diffraction the variations of the lattice parameters with temperature have been measured and compared with those of YCu_2. A magnetic ordering temperature at $T_N = 6.5 \pm 0.1$ K and a spin-reorientation temperature ($T_R = 4.1 \pm 0.1$ K) have been observed in the susceptibility, specific heat and resistivity. Further field-induced magnetic transitions around 1, 3 and 15 T (depending on the measuring temperature) were found in the magnetization and magnetoresistance. A preliminary magnetic phase diagram of $NdCu_2$ is presented. The crystal field excitation temperatures determined by inelastic neutron scattering experiments are $E_1/k_B = 34$ K, $E_2/k_B = 58$ K, $E_3/k_B = 84$ K and $E_4/k_B = 164$ K. For the determination of the nine crystal field parameters V_l^m the superposition model has been applied. The deduced set of parameters was used to calculate the crystal field influence on the magnetization, specific heat, thermal expansion and electrical resistivity. From an analysis of the x-ray powder diffraction data the lattice constants $a = 4.3844$ Å, $b = 7.0350$ Å and $c = 7.4186$ Å and the atomic positional parameters ($y_{Cu} = 0.0506$, $z_{Cu} = 0.1659$, $z_{Nd} = 0.5383$) inside the unit cell were obtained.

1. Introduction

In contrast to the large number of known rare-earth (R) 3d metal compounds which crystallize in the cubic Laves phase structure ($Fd3m$), the RCu_2 compounds (except $LaCu_2$) crystallize in the orthorhombic $CeCu_2$-type of structure with the space group $D_{2h}^{28}(Imma)$; $LaCu_2$ displays the hexagonal AlB_2-type of structure (Storm and Benson 1963). This lower symmetry of the Cu compounds may be the reason why this family of intermetallics is not so intensively investigated, although the magnetic properties of the RCu_2 had already been published by Sherwood *et al* (1964) in the 1960s. It is therefore a challenge to start a systematic investigation of this member of the '1:2

compounds' with lower symmetry, especially as previous investigations on polycrystalline and single crystal RCu_2 samples (Hashimoto *et al* 1979a,b) reveal that in most of these intermetallics one, or more, first- or second-order magnetic phase transitions exist below their ordering temperatures. These transitions are associated with changes in the magnetic structure (Lebech *et al* 1987). The magnetic structure as far as it has already been investigated appears to be complex, generally with an antiferromagnetic type of spin arrangement. It can be assumed that these transitions in the magnetic structure are at least partly caused by the crystal field influence on the R^{3+} ions, since $GdCu_2$ does not show any change in its magnetic structure.

The aim of the present article is twofold:

(i) to continue with the systematic investigation on the RCu_2 compound series which we have started with $CeCu_2$ (Gratz *et al* 1985) and $SmCu_2$ (Gratz *et al* 1990); and

(ii) to apply a recently developed theoretical concept (Newman 1983, Divis 1991) which allows us to deduce the proper crystal field parameters from inelastic neutron diffraction data in combination with other experimental results.

2. Sample preparation and experimental techniques

A polycrystalline sample of approximately 20 g has been obtained by induction melting in a protective argon atmosphere. After annealing at 700 °C for one week the phase purity has been checked by x-ray diffraction and metalographic methods. At least within the accuracy of these methods no traces of foreign phases have been found. Except for the neutron scattering experiments all the other investigations were performed on the same part of the melted sample.

A conventional Siemens D500 diffractometer with Co Kα radiation has been used for the measurements of the lattice constants as function of the temperature. The sample holder of the diffractometer has been replaced by an Oxford He-flow cryostat which operates in the temperature region from about 5 up to 500 K. The grain size of the powdered sample was smaller than 50 μm. After grinding the powder was heat treated at 400 °C for 5 h.

The inelastic neutron experiments have been performed at the IN6 and IN4 neutron time-of-flight spectrometers at ILL in Grenoble (details are given in section 3.2).

The magnetic measurements were done in a vibrating-sample magnetometer in fields up to 6.5 T and in the temperature range between 1.8 and 270 K.

The specific heat results have been obtained by means of an adiabatic calorimeter in the temperature range from 1.5–60 K. The calorimeter, employing the Nernst method of step heating, was calibrated and tested using pure Cu(99.999). The absolute accuracy is estimated to be better than 1% in the low temperature range and about 3% for $T > 30$ K.

For the thermal expansion a membrane technique was used. This method is based on the deformation of a Cu–Be–brass membrane on which a special kind of strain gauge is glued. Because of the brittleness of the RCu_2 sample, it cannot be excluded that there are microcracks in our spherically shaped sample used for the thermal expansion experiment. The estimated error in $\alpha(T)$ is about 10%.

The resistivity has been measured from 4.2 K up to nearly 1000 K using two different equipments, a bath-cryostat for the low-temperature region and an induction

furnace (with field compensation) above room temperature. In both cases a quasi-continuous 'four probe' measuring technique applied to bare-shaped samples was used. The uncertainty in the absolute value of the resistivity is determined by the uncertainty in the dimension of the specimen and is estimated to be about 5%. Although the experiments have been performed in high vacuum the oxidation of the sample was a serious problem at highest temperatures. Also in the case of thermopower two different apparatuses have been used. In both the low- and the high-temperature regions, a differential measuring method was used to determine the absolute thermopower. The magnitude of the gradient depends on the measuring temperature and was 0.1 K for the lowest temperature and increased up to about 10 K at the highest temperatures.

The thermal conductivity is studied up to room temperature. A steady-state measuring method was used. As a heater we used a strain gauge, which was glued on the one end of the sample. The temperature gradient produced by the heater was measured using a differential thermocouple fixed along the 30 mm long sample.

The magnetoresistance measurements ($\Delta\varrho/\varrho$) have been performed in a bath cryostat with an inserted superconducting coil. The highest field available was 13 T. The construction of the sample holder for the magnetoresistance enables the sample position to be changed relative to the magnetic field direction. The experimental data were obtained by measurements in the transversal position (transverse magnetoresistance).

3. Results and discussion

3.1. Structural investigation

We investigated the temperature dependence of the lattice parameters a, b and c of the *Imma*-type of structure in the temperature range from 4.2 up to 450 K and applied a refinement procedure to obtain the atomic positional parameters.

The lattice parameters at $T = 295$ K are $a = 4.3843 \pm 0.0004$ Å, $b = 7.0326 \pm 0.0006$ Å and $c = 7.4194 \pm 0.0015$ Å obtained in our low-temperature facility. These values are in agreement with the literature (Debray 1973) for a and c, while our b-value deviates from the literature value by about 0.4%. To check whether our values are reliable we prepared another $NdCu_2$ sample and repeated the lattice constant measurements at 295 K using the conventional room temperature sample holder. The values for a, b and c for the second sample are $a = 4.3844 \pm 0.0006$ Å, $b = 7.0350 \pm 0.0006$ Å and $c = 7.4186 \pm 0.0011$ Å. We feel that the reproducibility of these values is satisfactory as far as equipment and analysis of the data is concerned. Figure 1 shows the temperature dependence of the lattice constants in the temperature range from 4.2 up to 450 K (which is the highest temperature we can reach with our equipment) normalized to the values at 450 K. The lattice constants at 450 K are $a = 4.3917 \pm 0.0004$ Å, $b = 7.0579 \pm 0.0014$ Å and $c = 7.4392 \pm 0.0025$ Å. We obtained the lattice constants by monitoring the (112), (121), (022), (013), (031), (200), (103), (231), (134), (215) Bragg reflections with Co $K\alpha_1$ radiation, using germanium as an internal standard.

Figure 1 shows that the b-axis exhibits the strongest variation with temperature, whereas the a-axis variation is less pronounced. In particular, in the b-direction there are changes near 180 K while a further anomaly is observed below 30 K. For comparison the temperature variation of the lattice parameters of the isostructural YCu_2 compound is included in that figure. Clearly there is no such change in the variation with temperature for YCu_2. Since no crystal field influence in YCu_2 can be expected

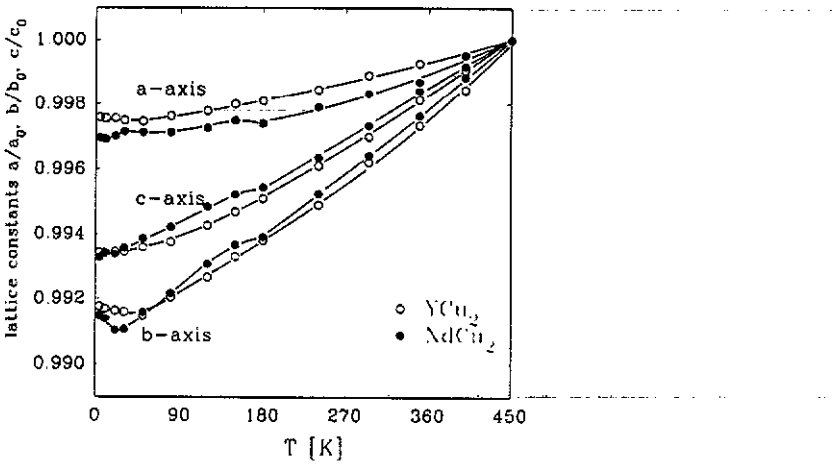

Figure 1. Temperature dependence of the lattice parameters a, b and c of $NdCu_2$ and YCu_2 normalized to 450 K.

we refer the differences in the temperature variation of the lattice parameters of YCu_2 and those of $NdCu_2$ (especially the pronounced minimum around 30 K) to the influence of the crystal field. It is not quite clear whether the anomaly observed below 180 K in all three directions (see figure 1) is also caused by the crystal field. It should be pointed out that the crystal field influence on the unit cell parameters was also observed in $SmCu_2$ (Gratz *et al* 1990) and in $ErCu_2$ (Gratz *et al* 1991). In section 3.5 we will show that in the thermal expansion experiments the influence of the crystal field is also clearly observable.

We now discuss the atomic positional parameters. The $CeCu_2$-type structure is body-centred orthorhombic (space group *Imma*) with four R atoms in the equivalent positions 4e: $(0, \frac{1}{4}, z)$, $(0, \frac{3}{4}, -z)$ and eight Cu atoms in 8h: $(0, y, z)$, $(0, -y, -z)$, $(0, \frac{1}{2} + y, -z)$, $(0, \frac{1}{2} - y, z)$. The positional parameters in this structure are z_{Nd}, y_{Cu} and z_{Cu}. The structure can be visualized as being built by stacking together sheets of Nd and Cu atoms in the sequence ABAB... along the a-axis direction. The layers are stacked such that adjacent layers are displaced relative to each other by the translation $(\frac{1}{2}, \frac{1}{2}, \frac{1}{2})$. In each layer, the R atoms form parallel zig-zag chains which are separated by the appropriate number of Cu atoms. Figure 2 shows the atomic arrangement in the $CeCu_2$ unit cell and its (100) layer for $NdCu_2$. For the experimental determination of z_{Nd}, y_{Cu} and z_{Cu} we used the single line crystal-structure refinement POWLS procedure (POWder Least Squares) (Will 1979). All together we analysed 26 x-ray profiles. The values for the atomic positional parameters of $NdCu_2$ are:

$$y_{Cu} = 0.0506 \pm 0.0024$$

$$z_{Cu} = 0.1659 \pm 0.0022$$

$$z_{Nd} = 0.5383 \pm 0.0017.$$

A secondary monochromator suppressed the Kβ lines and reduced the background radiation by more than 90%. The experiments have been performed at 295 $\pm$ 0.1 K keeping the temperature constant with a thermostat. X-ray reflections have been selected out of the 2Θ range from $2\Theta = 40°$ up to $2\Theta = 150°$. A preferred orientation,

which clearly exists in the (001) direction, has been taken into consideration. The R-value thus obtained is $R = 19.7\%$. The experimental and calculated intensities of the analysed x-ray line profiles are given in table 1. Details of the fit procedure will be published later.

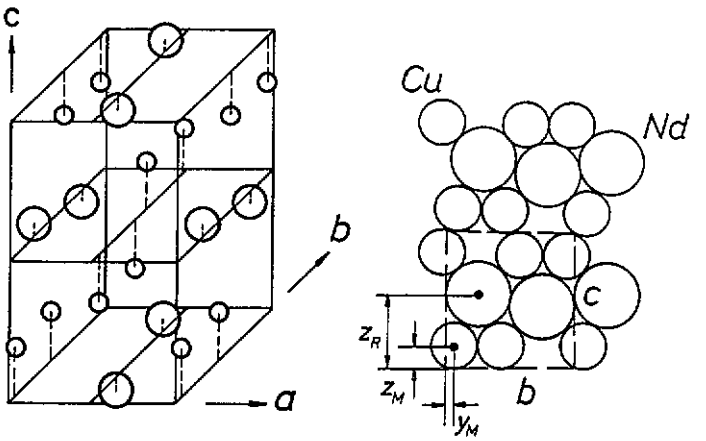

Figure 2. The unit cell of the $CeCu_2$-type structure (left) and the atomic arrangement of the Nd and Cu atoms in the b–c plane (right) is depicted. The atomic positional parameters for $NdCu_2$ obtained using the POWLS procedure are $y_{Cu} = 0.0506$, $z_{Cu} = 0.1659$ and $z_{Nd} = 0.5383$.

3.2. Inelastic neutron scattering

The experiments have been performed on a polycrystalline sample using the time-of-flight spectrometers IN4 and IN6 at the high-flux reactor of the Institute Laue–Langevin in Grenoble. Neutrons with incident energies of 12, 17 and 50 meV (IN4) and 3.17 meV (IN6) were used. All spectra were corrected for background, absorption and self-shielding and put on an absolute intensity scale by a standard vanadium calibration. Figures 3 and 4 show inelastic spectra for $NdCu_2$ in the low-Q region (averaged from 1 to 2 $Å^{-1}$) in the paramagnetic state at $T = 10$ K and in the magnetically ordered state below T_N, respectively. Magnetic scattering is the dominant contribution to the scattering intensity in the spectra (except for elastic scattering). The phonon scattering is negligible.

The obtained data were analysed with respect to the crystal field splitting of the $J = 9/2$ Hund's rule ground state and furthermore to the spin-dynamics in the ordered and paramagnetic states.

Let us first discuss the inelastic neutron spectra in the paramagnetic state at $T = 10$ K (figure 3). We observed four inelastic magnetic transitions which we interpret as crystal field transitions from the ground state level to excited crystal field levels at 34, 58, 84 and 164 K. The level scheme is shown as inset in figure 3. This is exactly what we expect for the Nd ion in orthorhombic symmetry: a splitting of the $J = 9/2$ Hund's rule ground state into five doublets. The data points for the three runs under different experimental conditions are in good agreement with respect to peak positions and absolute intensities. For clarity data points from the $E = 50$ meV run are only shown in the region around 15 meV, as the three-peak structure around 5 meV is seen in this run only as an unresolved shoulder to the elastic line due to the much poorer

Table 1. The measured and calculated intensities of the x-ray lines.

Miller indices	I_{cal} au	I_{obs} au
(112)	114	134
(121)	368	306
(022)	159	140
(013)	35	29
(031)	56	51
(103)	187	213
(040)	25	20
(033)	13	11
(222)+(114)	100	124
(024)	27	27
(141)+(213)+(042)	63	66
(231)	35	40
(015)	32	35
(301)	4	6
(051)+(134)	74	70
(240)	23	23
(143)	30	30
(233)	12	12
(312)	14	20
(321)	47	62
(224)	26	31
(125)	16	15
(242)	13	10
(152)+(303)+(035)	72	108
(215)	37	41
(037)	57	56

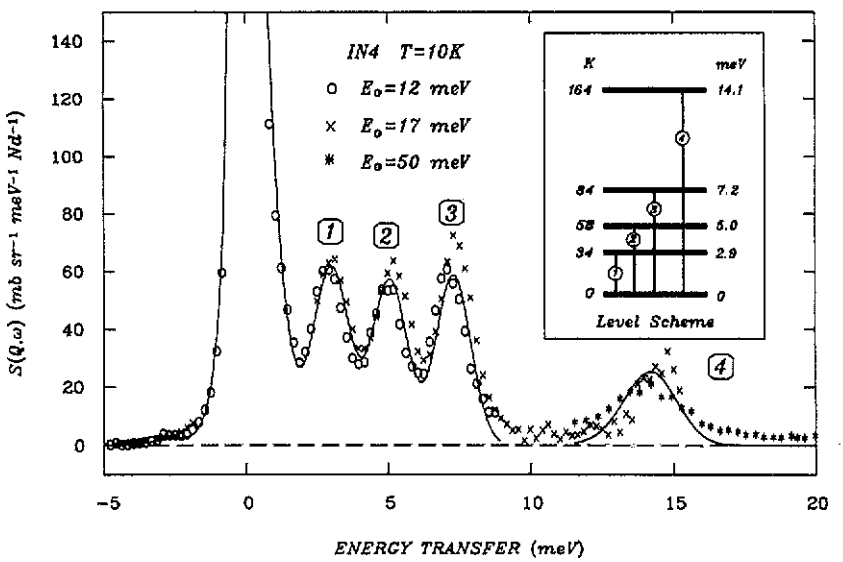

Figure 3. Inelastic neutron spectra in the paramagnetic state ($T = 10$ K) obtained with different incident neutron energies E_0. The deduced crystal field transitions are given by the level scheme in the inset. The nine crystal field parameters V_l^m have been obtained with the superposition model from these data (full curve).

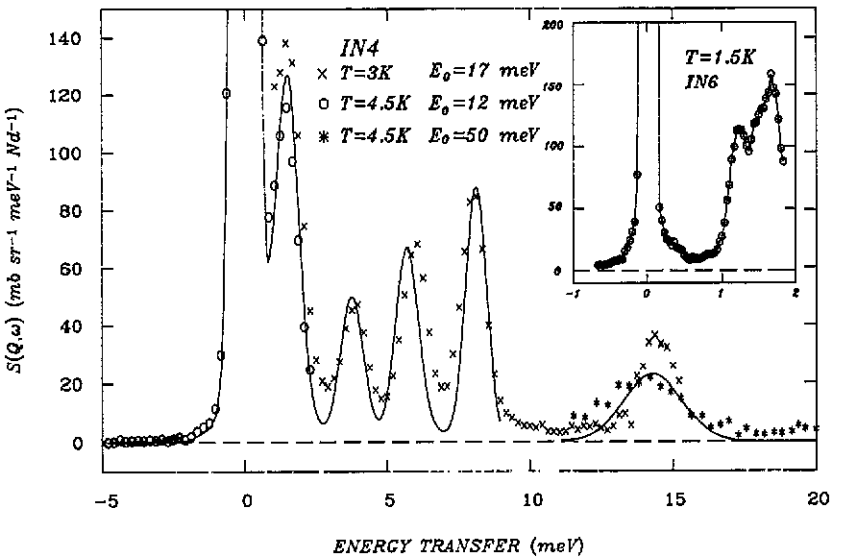

Figure 4. Inelastic neutron spectra at various temperatures below the Neèl temperature (= 6.5 K) obtained with different incident neutron energies. The inset shows the IN6 measurement at 1.5 K. The intensity in the energy range from 1–2 meV originates from magnon excitations.

resolution. The neutron scattering intensity has been fitted to the following formula:

$$S(Q,\omega) = NCg_J^2F^2(Q)\mathrm{e}^{-2W}\sum_{n,m}p_n\,|\langle n|J_\perp|m\rangle|^2\,\delta(\omega_{nm}-\omega) \tag{1}$$

with N the number of the magnetic atoms, $F(Q)$ magnetic form factor, p_n the thermal occupation probability and $J_\perp$ is the component of the total angular momentum operator perpendicular to Q. The other symbols have the usual meaning (Frick and Loewenhaupt 1986). The crystal field Hamiltonian for orthorhombic symmetry can be written in the Stevens parametrization scheme (Hutchings 1964):

$$\begin{aligned}H_{\mathrm{CF}} = {} & V_2^0O_2^0(J) + V_2^2O_2^2(J) + V_4^0O_4^0(J) + V_4^2O_4^2(J) + V_4^4O_4^4(J) \\ & + V_6^0O_6^0(J) + V_6^2O_6^2(J) + V_6^4O_6^4(J) + V_6^6O_6^6(J).\end{aligned} \tag{2}$$

Here V_l^m are the crystal field parameters and O_l^m are the operator equivalents. We observed that it is not convenient to fit the nine crystal field parameters directly without reliable starting values. One possible way to obtain promising starting crystal field parameters is to use the superposition model (SM), according to which the crystal field at the R site is given by the independent axially symmetric contribution from nearest ions (ligands) (Newman and Ng 1989). The model has been successfully used for R ions in insulators (Newman and Ng 1989). There are indications about its validity for intermetallic compounds, too (Newman 1983, Divis 1991). Using the assumptions of the SM the crystal field parameters in equation (2) can be written:

$$V_l^m = \alpha_l\sum_i k_{l,m}(i)\bar{A}_l(R_i). \tag{3}$$

Here α_l is the Stevens factor (Hutchings 1964) and $\bar{A}_l(R_i)$ are the so-called intrinsic parameters of the SM (Newman and Ng 1989). The coordination factors $k_{l,m}(i)$ of the ith neighbours shell are given by

$$k_{l,m}(i) = \sum_T S_m^l Z_m^l(\Theta_{T_i}, \Phi_{T_i}) \sqrt{\frac{4\pi}{2l+1}} \frac{1}{S_0^l} \tag{4}$$

where $Z_m^l(\Theta, \Phi)$ denotes tesseral harmonics (Hutchings 1964) and the numerical coefficients S_m^l/S_0^l are summarized by Newman and Ng (1989). The summation over T involves the angular coordinates Θ, Φ of the atoms from the ith equidistant coordination shell. In the case of $NdCu_2$ each Nd ion has twelve nearest Cu neighbours (the two, four, two, four in distances $R_1 = 2.99$ Å, $R_2 = 3.06$ Å, $R_3 = 3.14$ Å, $R_4 = 3.20$ Å). The six neighbouring Nd atoms lie at sufficiently larger distances ($R_{Cu}/R_R \simeq 0.848$) and we therefore neglect their contribution. The radial dependence of the intrinsic parameters was approximated by a power law $\bar{A}_l(R) = \bar{A}_l(R_0)(R_0/R_l)^{t_l}$. In ionic crystals $0 < t_l < 10$ holds. This constraint was also used in the earlier SM analysis of the crystal field in R intermetallics. With this in mind we have arbitrarily chosen a pair of t_4, t_6 to test the sensitivity of $\bar{A}_l(R_1)$ to the exponent t_l. Formulae 3 and 4 enable us to reduce the seven adjustable crystal field parameters V_l^m ($l > 2$) to the two adjustable intrinsic parameters $\bar{A}_4(R_1)$, $\bar{A}_6(R_1)$. It is well known that the second-order parameters V_0^2, V_2^2 cannot be satisfactorily described using SM (Newman and Ng 1989). On the other hand these parameters can be estimated from measurements of paramagnetic susceptibilities in single crystals as 0.8 and 1.1 K for V_2^0 and V_2^2, respectively (Hashimoto 1979a). Thus we started to fit the INS data in the two-parameter space $\bar{A}_4(R_1)$, $\bar{A}_6(R_1)$. The most promising sets of intrinsic parameters were found in the area $\bar{A}_4(R_1) > 0$, $\bar{A}_6(R_1) < 0$ and both the signs and magnitudes of the intrinsic parameters are not very sensitive to the value of the power-law exponent. After that we have used the corresponding crystal field parameters as starting parameters and allowed them to vary in order to fully account for the INS data. The best description of the experimental results has been obtained with the following set of crystal field parameters (see the full curve in figure 3):

$$V_2^0 = (1.35 \pm 0.06)\ \text{K} \qquad V_2^2 = (1.56 \pm 0.08)\ \text{K}$$
$$V_4^0 = (2.23 \pm 0.12) \times 10^{-2}\ \text{K} \qquad V_4^2 = (1.01 \pm 0.2) \times 10^{-2}\ \text{K}$$
$$V_4^4 = (1.96 \pm 0.42) \times 10^{-2}\ \text{K}$$
$$V_6^0 = (5.52 \pm 0.23) \times 10^{-4}\ \text{K} \qquad V_6^2 = (1.35 \pm 0.45) \times 10^{-4}\ \text{K}$$
$$V_6^4 = (4.89 \pm 0.43) \times 10^{-4}\ \text{K} \qquad V_6^6 = (4.25 \pm 0.19) \times 10^{-3}\ \text{K}.$$

This set of parameters also enables a satisfactory description of the crystal field influence of the magnetization, specific heat, thermal expansion and resistivity data (see later).

Let us finally discuss the inelastic neutron spectrum of $NdCu_2$ in the magnetically ordered state (figure 4). We observe a splitting of the ground state doublet and a shift of the peak positions of the crystal field transitions compared with the paramagnetic state. There is also a small difference in the spectra at medium energy transfers for

the measurements at 3 K ($E_0 = 17$ meV) and 4.5 K ($E_0 = 12$ meV). In a first approximation we can reproduce the inelastic spectrum at 3 K by adding to the single-ion crystal field Hamiltonian an internal magnetic field term $g_J \boldsymbol{J} \cdot \boldsymbol{H}_m$, using the crystal field parameters given previously and $H_m = 6.8$ T (full curve in figure 4). This simple model only yields a Zeeman splitting of the doublets in the ordered state. A measurement of the low-lying peak around 1.5 meV with the improved resolution of IN6 (inset in figure 4), however, reveals considerably more of the structure of this excitation. We may identify the intensity in the energy range from 1 to 2 meV as the magnon density-of-states of $NdCu_2$. The rather sharp drop of intensity below 1 meV possibly indicates a gap in the magnon excitation spectrum. This gap becomes smeared out if the measurements are performed at temperatures between T_R and T_N. This seems to be consistent with our observation that in this intermediate temperature region there is no longer a pure antiferromagnetic spin-arrangement, but the magnetic structure is now more complex. It is planned to continue the investigation of the magnetic structure and the spin wave dynamic on a single crystal in the near future. Finally it should be pointed out that we observed a Q-dependence of the intensity of the quasielastic line above T_N up to $T \simeq 20$ K indicative of short-range spin correlations. Such a conclusion has also been drawn from magnetization and specific heat experiments (see sections 3.3 and 3.4). The large negative magnetoresistance ($\Delta\varrho/\varrho$) values above T_N (up to about 25 K) supports this assumption, too (see section 3.6).

3.3. Magnetic measurements

The temperature dependence of the inverse susceptibility in the field of 0.07 T is given in figure 5. Above about 40 K a Curie–Weiss behaviour has been found, with a paramagnetic Curie temperature $\Theta = -8$ K and an effective moment of $\mu_{eff} = 3.38$ μ_B/Nd. The effective moment is reduced by about 6% compared with the theoretical value of 3.62 μ_B/Nd for the free $j = 9/2$ Nd^{3+} ion. Single crystal measurements reveal 3.53 μ_B/Nd (Hashimoto *et al* 1979a, Svoboda *et al* 1991). The inset in figure 5 shows the M against T behaviour in the low temperature region. The arrows mark the Neèl temperature ($T_N = 6.5 \pm 0.1$ K) and the spin-reorientation temperature ($T_R = 4.1$ K) as obtained from measurements without an external magnetic field (specific heat, resistivity). Figure 6 shows magnetization curves in fields up to 6.5 T for 2.1, 3.5, 4.2 and 8 K. For temperatures below T_R two field-induced magnetic transitions (as indicated by the shaded regions) appear in the field region of 6.5 T. Above the spin-reorientation temperature ($T_N > T > T_R$) the low-lying metamagnetic transition disappears, only the higher critical field exists in this intermediate temperature region. Recently performed magnetic measurements in pulsed magnetic fields up to 30 T indicate a further transition around 15 T (Bozukov *et al* 1991). Magnetization measurements on a single crystal reveal that these field-induced transitions are only observable in the b-direction, whereas in the c- and a-directions no transitions are visible in this field range (Hashimoto *et al* 1979a, Svoboda *et al* 1991). Note that the height of the step in M against H at 3 T is twice the increase in the magnetization at 1 T (see figure 6). Let us assume that the reason for the step-like changes in M against H are spin-flip transitions caused by the external field, it follows that in the transition at 3 T two times more spins must be involved in the spin-flip transition than in the transition at 1 T (because of the larger increase in M against H connected with the 3 T transition). We observed that the step height at the 15 T transition is the same as those at 1 T. Trying to sketch a tentative model for the spin arrangement in

the temperature region below 4.1 K, it has the following sequence in increasing fields. Starting from an antiferromagnetic spin arrangement of four spin down and four spin up in zero field, 1 T causes a flip of one spin into the field direction ('one spin flip'). A 'two spin flip' follows at 3 T, whereas the 15 T transition consists again of a 'one spin flip'. From the saturation of the magnetization curve we assume that a ferromagnetic spin arrangement in fields higher then 15 T is established. The saturation moment is 1.9 μ_B/Nd. In the intermediate temperature region ($T_N > T > T_R$) the situation concerning the spin arrangement seems to be more complex.

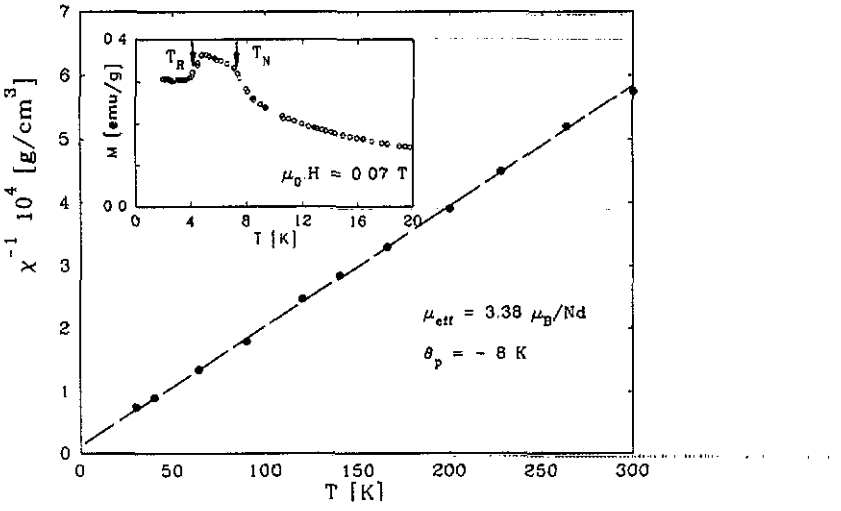

Figure 5. Inverse of the susceptibility against temperature. The inset shows the temperature dependence of the magnetization around T_R (spin-reorientation temperature = 4.1 K) and T_N (Neèl temperature = 6.5 K).

It is noteworthy that the magnetization curves above T_N show quite pronounced curvatures up to temperatures near 30 K. Figure 6 includes as an example the M against H curve at 8.1 K. Since such a curvature can be caused by the crystal field influence we calculated the field dependence of the magnetization for several temperatures using only the crystal field interaction (full curve in figure 6 shown for 8.1 K). As it can be seen from figure 6 it is clear that the crystal field influence alone does not fully describe the M against H behaviour at 8.1 K. But if magnetic correlation interactions are additionally taken into account (we already claimed short-range magnetic correlations from the neutron diffraction data) the M against H behaviour can be satisfactorily explained (see the broken curve in figure 6). A preliminary phase diagram of $NdCu_2$ will be discussed in our conclusion at the end of this article.

3.4. Specific heat

In figure 7 the temperature dependence of the specific heat of $NdCu_2$ and of the non-magnetic isostructural $LuCu_2$ are presented up to about 50 K. The inset shows details of c against T in the lower temperature region. From this measurement T_N has been determined as (6.5 ± 0.1 K) and the spin-reorientation temperature as 4.1 K.

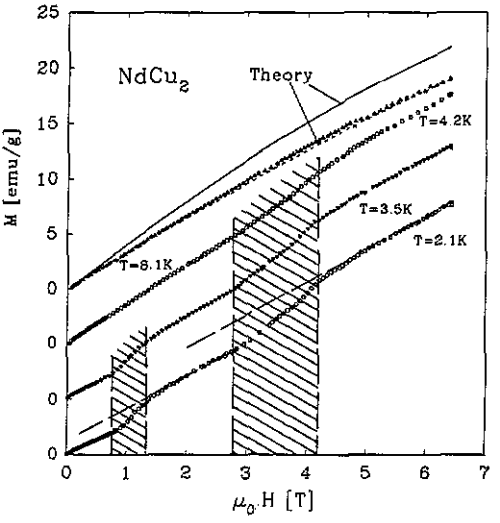

Figure 6. Magnetization curves in fields up to 6.5 T at various temperatures. The shaded areas indicate two critical field regions where field-induced magnetic transitions take place. The full and the broken curves give the calculated magnetization curves (crystal field only, full curve; crystal field plus correlation effects, broken curve).

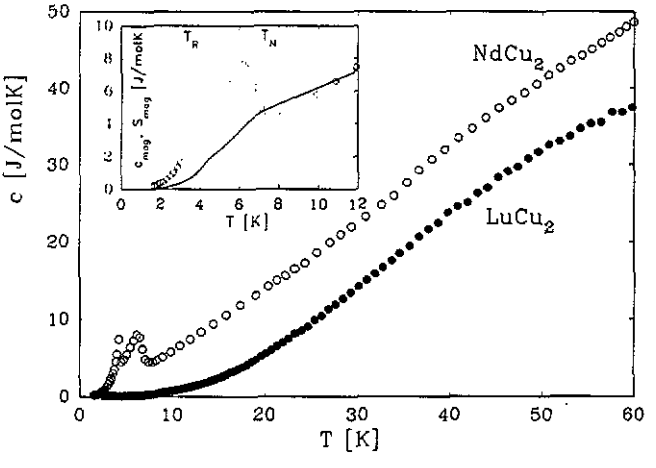

Figure 7. Temperature dependence of the specific heat of $NdCu_2$ and $LuCu_2$. The inset gives the specific heat at the lowest temperatures with T_R (= 4.1 K, spin-reorientation temperature) and T_N (= 6.5 K, Neèl temperature). In the inset the magnetic entropy against temperature is also depicted.

The temperature dependence of the specific heat $c(T)$ can be described at low temperatures by

$$c(T) = \gamma T + \beta T^3 + c_{\mathrm{mag}}(T) + c_{\mathrm{nucl}}(T) \tag{5}$$

with γT and βT^3 being the electronic and the phonon contribution to the specific heat, respectively. From a c/T against T^2 plot the γ coefficient was estimated to be around 8–12 mJ(mol K^2)$^{-1}$. The estimate of the γ value is to some extent uncertain

as the magnetic contribution in the ordered state and the correlations exist in a rather extended range above T_N. However, this value of $\simeq 10$ mJ(mol K^2)$^{-1}$ is comparable with $\gamma(TmCu_2) = 9$ mJ(mol K^2)$^{-1}$ (Sima *et al* 1988) and $\gamma(YCu_2) = 6.7$ mJ(mol K^2)$^{-1}$ (Luong *et al* 1985). The γ value of $SmCu_2$ is about twice as high (Gratz *et al* 1990) and that of $CeCu_2$, which is a Kondo system, is more than eight times higher than the γ value of $NdCu_2$ (Gratz *et al* 1985).

c_{mag} represents the magnetic and c_{nucl} the nuclear part of the total specific heat. c_{nucl} is only observable at very low temperatures and can therefore be neglected in our case. For a quantitative determination of c_{mag} we assumed that the phonon and conduction electrons contributions are the same as in non-magnetic $LuCu_2$. We therefore deduced c_{mag} as

$$c_{mag} = c(NdCu_2) - c(LuCu_2). \tag{6}$$

The obtained temperature variation of c_{mag} is given in figure 8. The contribution c_{mag} does not vanish above T_N, but shows a broad and pronounced maximum around about 20 K. In this figure we also included the position of the Schottky anomaly as obtained with the previously given crystal field eigenvalues E_i (see section 3.2) according to a model developed by Barron *et al* (1980):

$$c_{CF} = \frac{Z\sum_i E_i^2 \exp(-E_i/k_BT) - [\sum_i E_i \exp(-E_i/k_BT)]^2}{k_BT^2Z^2} \tag{7}$$

(Z is the partition function). Clearly, the curvature of c_{mag} above T_N is related to the crystal field influence, but there are hints to correlations between the Nd 4f moments, because of the difference between the experimental data and the Schottky peak obtained from the calculation. The temperature variation of the magnetic entropy was calculated from

$$S_{mag} = \int \frac{c_{mag}}{T}\,dT. \tag{8}$$

c_{mag} (symbols) together with S_{mag} (full curve) against T are plotted in the inset of figure 7. It can be seen that S_{mag} does not reach the theoretical value of $R\ln 2$ at T_N, as one would expect for a complete removal of the two-fold spin-degeneracy of the crystal field ground state doublet. It is noteworthy that a similar reduction of S_{mag} was found for $CeCu_2$ but not for $SmCu_2$ (Gratz *et al* 1990). There are mainly two possibilities explaining such a reduction of the entropy:

(i) pronounced short-range correlation effects in the paramagnetic phase; and/or

(ii) a substantial Kondo derived reduction of the R moments, as in the $CeCu_2$-compound. In the present case of $NdCu_2$ the influence of the short-range correlations seem to be more likely as the reason for the reduced entropy value.

3.5. Thermal expansion

Previous investigations of the thermal expansion, $\alpha(T)$, in $ErCu_2$ (Franse *et al* 1985), $TmCu_2$ (Sima *et al* 1988) and $SmCu_2$ (Gratz *et al* 1990) showed that the crystal field influence in the paramagnetic state reveals characteristic minima in α against T.

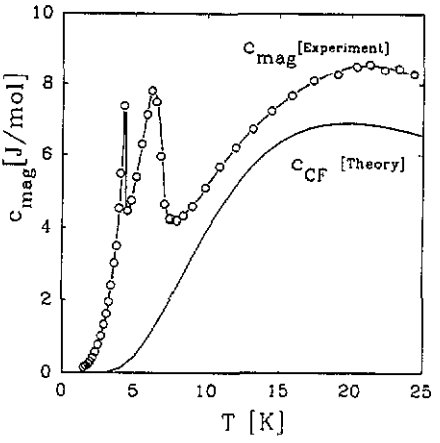

Figure 8. The temperature dependence of the magnetic contribution to the specific heat c_{mag} is shown together with the calculated Schottky anomaly as obtained by using the crystal field eigenvalues E_i from the neutron experiment.

As for the specific heat, the spin-dependent contribution to the thermal expansion $\Delta\alpha(T)$ was deduced by comparing the thermal expansion of $NdCu_2$ (magnetic) and $LuCu_2$ (non-magnetic). This analysis is based on the following assumptions:

$$\alpha(NdCu_2) = \alpha_e(T) + \alpha_{ph}(T) + \Delta\alpha(T) \tag{9}$$

$$\alpha(LuCu_2) = \alpha_e(T) + \alpha_{ph}(T) \tag{10}$$

where α_e denotes the electronic, α_{ph} the phonon and $\Delta\alpha$ the spin-dependent contributions to the total thermal expansion. Subtracting $\alpha(LuCu_2)$ from $\alpha(NdCu_2)$ we obtain $\Delta\alpha(T)$, with

$$\Delta\alpha(T) \simeq \alpha_{mag}(T) + \alpha_{CF}(T). \tag{11}$$

α_{mag} denotes the contribution due to spin correlations either in the ordered state (below T_N) or in the paramagnetic state, (where short-range correlations have been observed). α_{CF} is the crystal field induced part of the thermal expansion.

Since the crystal field parameters of the $^4I_{9/2}$ ground state multiplet are known we can calculate the temperature variation of $\alpha_{CF}(T)$. This calculation is based on the model for the magnetoelastic interaction described in detail by Divis *et al* (1990). In the framework of this model α_{CF} is related to the mean values of the second-order operators $\langle O_2^0(J)\rangle$ and $\langle O_2^2(J)\rangle$ as

$$\alpha_{CF} = \frac{1}{k_B T^2}\left\{A\left(\langle O_2^0 E\rangle - \langle O_2^0\rangle\langle E\rangle\right) + B\left(\langle O_2^2 E\rangle - \langle O_2^2\rangle\langle E\rangle\right)\right\} \tag{12}$$

where A and B are functions of the magnetoelastic coefficients and elastic constants (Divis *et al* 1990).

Using the experimental data, $\Delta\alpha$ can be obtained by subtracting $\alpha(LuCu_2)$ from $\alpha(NdCu_2)$. $\Delta\alpha(T)$ is given in figure 9 by the symbols.

Assuming for the moment that in the paramagnetic temperature region $\Delta\alpha \simeq \alpha_{CF}$ (i.e. we neglect the contribution due to the short-range correlations) we may now compare both quantities $\Delta\alpha$ and α_{CF}.

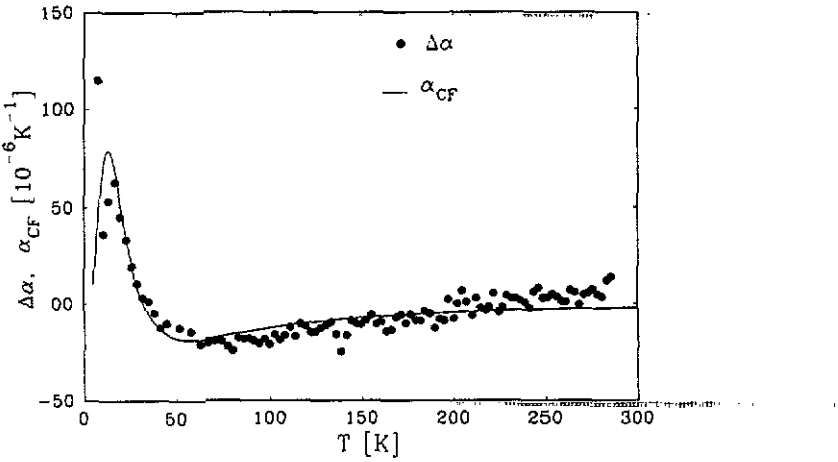

Figure 9. The temperature variation of the spin-dependent contribution to the thermal expansion is given by the symbols. The full curve shows the calculated influence of the crystal field on the thermal expansion.

A fit using equation (12) with the two adjustable parameters A and B was performed. The agreement between the experimental deduced $\Delta\alpha$ and calculated $\alpha_{CF}(T)$ can be seen from figure 9, where the theoretical result is presented by the full curve. The values for the coefficients $A(= -4.8 \times 10^{-5})$, $B(= -1.6 \times 10^{-4})$ can be scaled by second-order Stevens factors α_2 to compare with those obtained earlier from a similar analysis in $TmCu_2$ (Divis *et al* 1991). We have found that the coefficient A/α_2 has the same sign and roughly the same magnitude while B/α_2 changes sign when going from $NdCu_2$ to $TmCu_2$, respectively. The slightly deviating behaviour of $\Delta\alpha$ and α_{CF} is probably due to the neglection of α_{mag} in our calculation.

3.6. Transport properties

3.6.1. Electrical resistivity. The temperature dependence of the electrical resistivity $\varrho(T)$ of $NdCu_2$ is given in figure 10. The two observed kinks in ϱ against T at low temperatures (see the inset in figure 10) indicate the Neèl temperature T_N (at 6.5 ± 0.2 K) and the spin-reorientation temperature T_R slightly above 4 K (4.1 ± 0.2 K). These values have been determined from a $d\varrho/dT$ against T plot.

Assuming the validity of Matthiessen's rule the total electrical resistivity is given by

$$\varrho(T) = \varrho_o + \varrho_{ph}(T) + \varrho_{mag}(T) \tag{13}$$

where ϱ_o, ϱ_{ph} and ϱ_{mag} denote the residual, the phonon and the magnetic (spin-dependent) contribution, respectively. The two kinks mentioned previously, originate from the contribution ϱ_{mag}, which develops if the arrangement of the localized 4f moments changes. This is the case at T_N, since the long-range magnetic order collapses, whereas at T_R the antiferromagnetic arrangement of the spins (existing below T_R) changes to a kind of ferrimagnetism. In the simplest case ϱ_{mag} is temperature independent above T_N, but the influence of the crystal field level population can give rise to a temperature dependence of ϱ_{mag}.

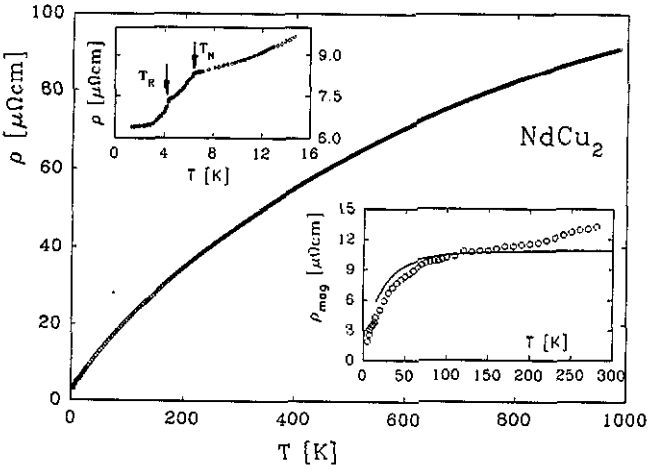

Figure 10. Temperature dependence of the electrical resistivity of $NdCu_2$. The two insets show the Neèl and the spin-reorientation temperature (upper left). ϱ_{mag} from experiment (given by the symbols) and the calculated ϱ_{mag} (given by the full curve) is shown in the second inset.

The temperature variation of ϱ_{mag} can be determined experimentally by comparing the $\varrho(T)$ of $NdCu_2$ with $\varrho(T)$ of one of the non-magnetic isostructural compounds. For that purpose we used YCu_2 (since the phase purity and the mechanical quality of our YCu_2 resistivity sample was excellent). After subtracting the residual resistivities from both ϱ against T curves, the assumption was made that $\varrho_{ph}(T)$ is similar for both compounds. The thus obtained temperature variation of ϱ_{mag} above T is plotted in the second inset of figure 10. The tendency to increase slightly of the experimentally determined ϱ_{mag} is probably due to differences in ϱ_{ph} for the two compounds. However the curvature due to the crystal field level population appears exactly in the same temperature region as given by the theoretical analysis (given by the full curve in the inset of figure 10). For the theoretical calculation we used the following expression:

$$\varrho_{mag}(T > T_N) = A \sum_{n,m} |\langle n|\boldsymbol{s}\cdot\boldsymbol{J}|m\rangle|^2 p_n f_{nm} \tag{14}$$

with the thermal occupation probability

$$p_n = \frac{\exp(-E_n/k_B T)}{\sum_m \exp(-E_m/k_B T)} \tag{15}$$

and the Fermi factor f_{nm}. The constant A contains several factors such as the exchange coupling constant or the Fermi energy (for more details see Gratz and Zuckermann 1982).

In connection with $\varrho(T)$ there is another interesting observation, concerning the pronounced negative curvature in the higher temperature region up to 1000 K. Usually it is assumed that for temperatures larger than the Debye temperature ϱ_{ph} (which is theoretically described by the Bloch–Grüneisen law) causes a linear temperature dependence of ϱ. But this could not be found in our experiment (ϱ_{mag} is temperature independent above the temperature region where all the crystal field levels are occupied). We suppose that this negative curvature in the temperature variation of the resistivity is connected with band structure effects (Allen 1972).

3.6.2. Thermopower. The temperature dependence of the thermopower $S(T)$ of $NdCu_2$ is given in figure 11. A comparison of the temperature variation of S of $NdCu_2$ and $SmCu_2$ (Gratz *et al* 1990) reveals remarkable similarities for the temperature region below room temperature, but at high temperatures $NdCu_2$ behaves differently. The S against T curve for $SmCu_2$ increases continously up to 1000 K with a tendency towards weak saturation, whereas the S against T curve for $NdCu_2$ goes through a maximum around 600 K and at about 850 K a change of sign takes place.

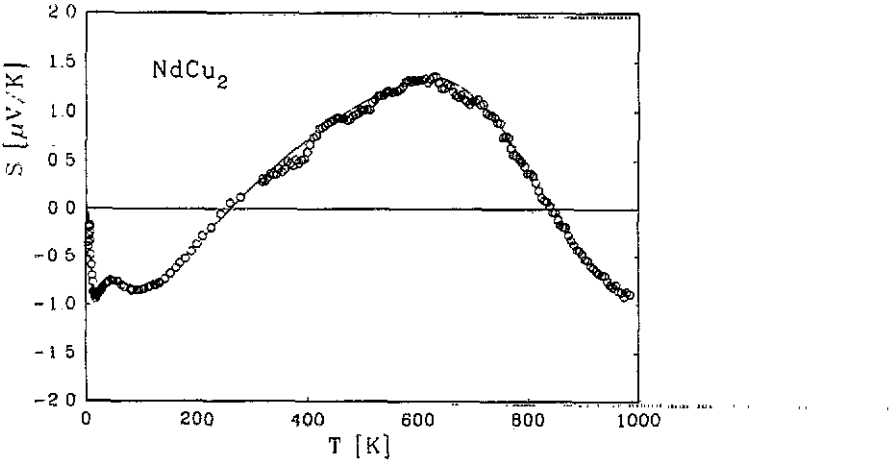

Figure 11. Temperature dependence of the thermopower of $NdCu_2$.

Instead of Matthiessen's rule, the Nordheim–Gorter rule has to be used for thermopower when taking the different scattering processes into account (see, e.g., Gratz and Nowotny 1985). The Nordheim–Gorter rule enables the different scattering contributions to be separated (due to potential scattering, phonon scattering and spin-dependent scattering processes). Measurements of S against T for all the RCu_2 compounds below room temperature unequivocally show that spin-dependent scattering processes influence the total thermopower in a characteristic way (Gratz and Zuckermann 1982). With respect to the crystal field influence Fulde (1978) showed that the crystal field can give rise to a maximum or a minimum in $S(T)$. The position of the minimum or maximum depends on an overall crystal field splitting. In $NdCu_2$ the crystal field influence on the temperature variation of the thermopower is at least partly responsible for the complex temperature variation below 200 K. Although it is known that minima in S against T at temperatures around 10–50 K can be caused by the phonon-drag effect, we assume that the weak minimum near 80 K is due to the crystal field. Note that the position of the minimum coincides with the temperature region where in resistivity the large crystal field induced curvature of ϱ_{mag} is observed.

Recently performed theoretical investigations revealed that the sign and shape of $S(T)$ in the high temperature region give an impression of what the density of states $N(\varepsilon)$ near to the Fermi energy would look like. Following our results (Brunner 1990) the positive sign and maximum in S against T in the high temperature region can be understood if the Fermi energy is situated on the left-hand side of a minimum in $N(\varepsilon)$. To our knowledge no band structure calculations exist for $NdCu_2$, but there are calculations for YCu_2 (Harima *et al* 1990). These calculations for YCu_2 showed that the Fermi level is on the left-hand side of a local minimum in $N(\varepsilon)$. Under

the assumption that the band structure calculations will not differ very much for isostructural compounds we can predict that in $NdCu_2$ the Fermi energy is also on the left-hand side of a minimum in $N(\varepsilon)$. Since the curvature of $S(T)$ is much more pronounced for $NdCu_2$ in this high temperature region this local minimum should be much narrower in the $N(\varepsilon)$ of $NdCu_2$. It would be interesting to confirm this prediction by band structure calculations.

3.6.3. Thermal conductivity. In figure 12 the temperature variation of the thermal conductivity λ for $NdCu_2$ in the range from 4.2 up to 300 K is depicted. For comparison a plot of λ against T for isostructural non-magnetic YCu_2 is included. There is a striking difference between the two $\lambda(T)$ curves presented in figure 12. This cannot simply be referred to magnetic scattering processes which exist in $NdCu_2$ but not in YCu_2. The maximum in $\lambda(T)$ observed for YCu_2 is mainly due to the much lower potential scattering rate. (Note: The residual electrical resistivity of YCu_2 is about 1 $\mu\Omega$ cm compared to 6.5 $\mu\Omega$ cm for $NdCu_2$ (ϱ_o is a direct measure of the potential scattering)).

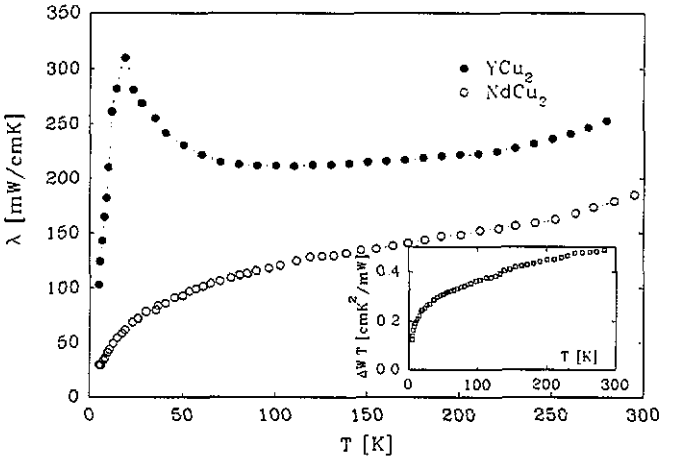

Figure 12. Temperature dependence of the thermal conductivity (λ) of $NdCu_2$ and YCu_2. The inset shows ΔWT against T deduced from $[1/\lambda(NdCu_2)-1/\lambda(YCu_2)]$ data.

To figure out the influence of the crystal field on the thermal conductivity a careful analysis of the $\lambda(T)$ data is necessary. In the following we will show that the crystal field influence is also visible in this transport property. For that we make use of the procedure presented in an article by Bauer *et al* (1986).

Generally it is assumed that the total thermal conductivity is given by the sum of two contributions:

$$\lambda = \lambda_e + \lambda_g \tag{16}$$

where λ_e and λ_g are the electronic and the lattice thermal conductivities, respectively. Under the assumptions: (i) λ_g is negligible compared with λ_e; and (ii) the Matthiessen rule is applicable to the electronic thermal conductivity, the total thermal resistivity

of the non-magnetic (NM) YCu_2 and of the magnetic (M) $NdCu_2$ is given by

$$\frac{1}{\lambda^{NM}} \simeq W_e^{NM} = W_{e,o}^{NM} + W_{e,ph}^{NM} \tag{17}$$

$$\frac{1}{\lambda^{M}} \simeq W_e^{M} = W_{e,o}^{M} + W_{e,ph}^{M} + W_{e,mag}^{M}. \tag{18}$$

The subscripts (e, o) and (e, ph) denote scattering processes of conduction electrons by static imperfections (potential scattering) and by phonons, respectively. To deduce the spin-dependent scattering contribution $W_{e,mag}$ we subtract the two equations (17) and (18):

$$\Delta W = W_e^{M} - W_e^{NM} = (W_{e,o}^{M} - W_{e,o}^{NM}) + (W_{e,ph}^{M} - W_{e,ph}^{NM}) + W_{e,mag}^{M}. \tag{19}$$

Assuming that $W_{e,ph}^{M}$ and $W_{e,ph}^{NM}$ are equal for the two isostructural compounds it follows that

$$\Delta W \simeq (W_{e,o}^{M} - W_{e,o}^{NM}) + W_{e,mag}^{M}. \tag{20}$$

Theoretically it has been shown that the thermal residual resitivity $W_{e,o}$ is proportional to $1/T$ (Klemens 1969), recently we could demonstrate that; $W_{e,mag}$, in the paramagnetic temperature region, is also a function of $1/T$ and is given by (Bauer *et al* 1986)

$$W_{e,mag} = C(g-1)^2 J(J+1)(1/T) \tag{21}$$

C is a constant, $(g-1)^2 J(J+1)$ is the de Gennes factor. This relationship only holds as long as there is no crystal field influence. ΔW can now be written as

$$\Delta W = (B^{M} - B^{NM}) \frac{1}{T} + [C(g-1)^2 J(J+1)] \frac{1}{T} \tag{22}$$

where B^{M} and B^{NM} are related to ϱ_o via the Wiedemann–Franz law.

Experimentally the values for ΔW have been obtained from the difference $(1/\lambda^{M} - 1/\lambda^{NM})$, where λ^{NM} is the thermal conductivity of YCu_2.

According to equation (22) ΔWT is temperature independent as long as the assumptions mentioned previously are fullfiled, i.e. $W_{e,ph}^{M} = W_{e,ph}^{NM}$ and if there is no crystal field influence on $W_{e,mag}$. However, if there is a crystal field influence it causes a curvature of ΔWT. The inset in figure 12 depicts ΔWT against temperature. As can be seen there is a pronounced curvature below 80 K. This is attributed to the crystal field influence for the following reasons:

(i) The curvature in the plot of ϱ_{mag} against T (which is due to the crystal field), is in the same temperature region. Such a comparison can certainly be made, because the physical origin of $W_{e,mag}$ and ϱ_{mag} are the same.

(ii) If we apply this kind of analysis to $GdCu_2$ we do not detect such curvature (there is no crystal field effect in the Gd compound). The observation that ΔWT does not become temperature independent above this curved region is probably because $W_{e,ph}^{M}$ is not exactly the same as $W_{e,ph}^{NM}$ which we assumed in our analysis.

3.7. Magnetoresistance

The magnetoresistance of magnetic metals is an interesting phenomena in which transport properties couple with magnetism. There are several reasons for the appearence of the magnetoresistance. Firstly, there is the change of the scattering mechanism because an external magnetic field influences the dynamic of the localized spins. Secondly, a change of the carrier number, i.e. a change of the band structure can take place under the influence of an external magnetic field. The magnetoresistance is defined by

$$\Delta\varrho/\varrho = \frac{\varrho(H) - \varrho(0)}{\varrho(0)}. \tag{23}$$

Yamada and Takada (1973a) showed that the magnetoresistance in antiferromagnetic metals is *positive* for the case of weak magneticfields, i.e. $\tau\omega_H \ll 1$, where τ is the relaxation time of the conduction electrons and ω_H is the cyclotron frequency. In the ferro- and paramagnetic case the external field increases the effective field acting on the localized spins and suppresses the fluctuation of the localized spins leading to a *negative* magnetoresistance. In a following article (Yamada and Takada 1973b) these authors showed that a positive peak in $\Delta\varrho/\varrho$ appears at the critical field, if an antiferromagnetic or ferrimagnetic spin arrangement changes under the influence of the field.

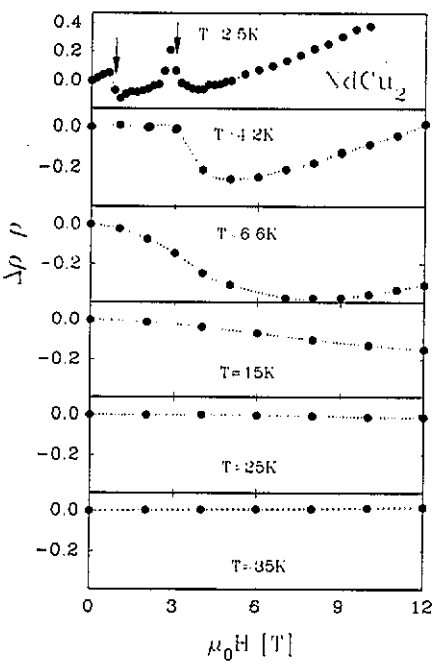

Figure 13. Field dependence of the magnetoresistance ($\Delta\varrho/\varrho$) at T = 2.5, 4.2, 6.6, 15, 25 and 35 K. The two arrows indicate two field induced magnetic transitions at 1 and 3 T.

In figure 13 we present $\Delta\varrho/\varrho$ against the external magnetic field $\mu_0 H$ up to 12 T for different temperatures. Depending on whether the temperature is selected below

T_R or in $T_R < T < T_N$ or above T_N, very different kinds of $\Delta\varrho/\varrho$ against H dependences are observed. A two-peak structure exists at 2.5 K indicating that up to 12 T two magnetic transitions can be induced by the field. This is exactly what we have already found in our magnetic investigations (see section 3.3). According to the calculation by Yamada and Takada (1973b) fluctuating moments just below and above the magnetic instabilities are responsible for the peak structure. In the temperature range $T_R < T < T_N$ the two-peak structure disappears. The low-lying field induced transition at $H = 1$ T is now suppressed. The higher transition at 3 T still exists but now a drop of $\Delta\varrho/\varrho$ towards large negative values is measured in fields higher than 3 T. We refer that observation to the now dominating ferromagnetic kind of spin arrangement. The very large negative magnetoresistance just above the Neèl temperature is connected with short-range correlations which we already claimed from neutron, magnetization and specific heat investigations. Following the $\Delta\varrho/\varrho$ measurements in the higher temperature region it appears that these correlations become suppressed by the temperature. They finally disappear above 30 K. The $\Delta\varrho/\varrho$ against H plots above 35 K up to 300 K show a slightly positive magnetoresistance increasing with temperature.

4. Conclusion

Summarizing the most substantial results of the present article, we may say that

(i) The crystal field level scheme of Nd^{+3} in $NdCu_2$ deduced from inelastic neutron scattering data is: $E_1/k_B = 34$ K, $E_2/k_B = 58$ K, $E_3/k_B = 84$ K and $E_4/k_B = 164$ K.

(ii) The crystal field parameters obtained from the inelastic neutron spectra within the scope of the superposition model are:

$$V_2^0 = (1.35 \pm 0.06)\ \text{K} \qquad V_2^2 = (1.56 \pm 0.08)\ \text{K}$$

$$V_4^0 = (2.23 \pm 0.12) \times 10^{-2}\ \text{K} \qquad V_4^2 = (1.01 \pm 0.2) \times 10^{-2}\ \text{K}$$

$$V_4^4 = (1.96 \pm 0.42) \times 10^{-2}\ \text{K}$$

$$V_6^0 = (5.52 \pm 0.23) \times 10^{-4}\ \text{K} \qquad V_6^2 = (1.35 \pm 0.45) \times 10^{-4}\ \text{K}$$

$$V_6^4 = (4.89 \pm 0.43) \times 10^{-4}\ \text{K} \qquad V_6^6 = (4.25 \pm 0.19) \times 10^{-3}\ \text{K}.$$

This set of parameters is capable of describing the crystal field influence on the susceptibility, specific heat, thermal expansion and electrical resistivity.

(iii) In magnetization and magnetoresistance measurements we observed that below $T_N = 6.5$ K a temperature induced magnetic transition from an antiferromagnetic to a kind of ferrimagnetic rearrangement of the spins takes place at $T_R = 4.1$ K. Below T_R $NdCu_2$ undergoes two field induced magnetic transitions up to 12 T. A further transition around 15 T into a ferromagnetic polarized state can be deduced from high field experiments performed at 4.2 K. In figure 14 we have collected our ideas concerning a magnetic phase diagram and our suggestions as to how the spin arrangements in the various kinds of magnetic states might look, although neutron diffraction experiments on a single crystal, which are now in preparation, are necessary to confirm our ideas.

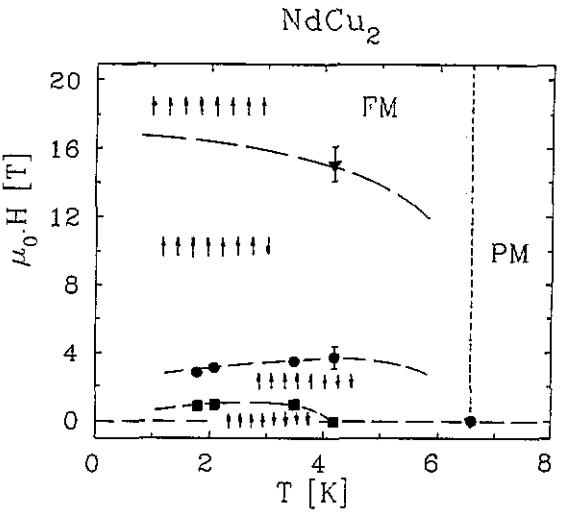

Figure 14. A proposed phase diagram for $NdCu_2$. The arrows indicate possible spin alignment in the various magnetic ordered regions.

Acknowledgments

We thank our colleagues St Pöllinger, A Lindbaum and M Rotter for very fruitful experimental cooperation.

Several parts of this work have been supported by the Austrian Science Foundation: Transport Properties Project No. P7994-TEC, Specific Heat Project No. P7918-TEC.

We also thank the Hochschuljubiläumsstiftung der Stadt Wien for financial support.

References

Allen Ph 1972 *Phys. Rev.* B **6** 2577

Barron T H K, Collins J G and White G K 1980 *Adv. Phys.* **29** 609

Bauer E, Gratz E and Adam G 1986 *J. Phys. F: Met. Phys.* **16** 493

Bozukov L, Gilewski A and Gratz E 1991 *Proc. 3rd Conf. on High Magnetic Fields (Amsterdam, 1991), Physica* B at press

Brunner H 1990 *PhD Thesis* Technische Universtät Vienna, Austria

Debray D 1973 *J. Less-Common. Met.* **30** 237

Divis M 1991 *Phys. Status Solidi* b **164** 227

Divis M, Lukáč P and Svoboda P 1990 *J. Phys.: Condens. Matter* **2** 7569

Franse J J M, Luong N H and Hien T D 1985 *J. Magn. Magn. Mater.* **50** 153

Frick B and Loewenhaupt M 1986 *Z. Phys. B: Condens. Matter* **63** 207

Fulde P 1978 *J. Appl. Phys.* **49** 1311

Gratz E, Bauer E, Barbara B, Zemirli S, Steglich F, Bredl C D and Lieke W 1985 *J. Phys. F: Met. Phys.* **15** 1975

Gratz E, Loewenhaupt and Divis 1991 unpublished

Gratz E and Nowotny H 1985 *Physica* B **30** 205

Gratz E, Pillmayr N, Bauer E, Müller H, Barbara B and Loewenhaupt M 1990 *J. Phys.: Condens. Matter* **2** 1485

Gratz E and Zuckermann M J 1982 *Handbook on the Physics and Chemistry of Rare Earth* vol 5, ed K A Gschneidner Jr and L Eyring (Amsterdam: North-Holland) ch 42, p 117

Harima H, Miyahara S and Yanase A 1990 *Physica* B **163** 205

Hashimoto Y, Fujii H, Fujiwara H and Okamoto T 1979a *J. Phys. Soc. Japan* **47** 67
—— 1979b *J. Phys. Soc. Japan* **47** 73
Hutchings M T 1964 *Solid State Physics* vol 16, p 227
Klemens P G 1969 *Thermal Conductivity* vol 1, ed R P Tye (London: Academic) p 35
Lebech B, Smetana Z and Sima V 1987 *J. Magn. Magn. Mater.* **70** 97
Luong N H, Franse J J M and Hien T D 1985 *J. Magn. Magn. Mater.* **50** 153
Newman D J 1983 *J. Phys. F: Met. Phys.* **13** 1511
Newman D J and Ng B 1989 *Rep. Prog. Phys.* **52** 699
Sherwood R C, Williams H J and Wernick J H 1964 *J. Appl. Phys.* **35** 1049
Sima V, Smetana Z, Divis M, Svoboda P, Zajac Š, Bischof D, Lebech B and Kayzel F 1988 *J. Physique Coll.* **49** C8 415
Storm A R and Benson K E 1963 *Acta Crystallogr.* **16** 701
Svoboda P, Divis M, Andreev A U, Baranov N and Markin P 1991 *J. Magn. Magn. Mater.* accepted for publication
Will G 1979 *J. Appl. Crystallogr.* **12** 483
Yamada H and Takada S 1973a *J. Phys. Soc. Japan* **34** 51
—— 1973b *Prog. Theor. Phys.* **49** 1401